Low-temperature growth morphology of singular and vicinal Ge(001)

Joseph E. Van Nostrand,* S. Jay Chey,† and David G. Cahill
Department of Materials Science and Engineering, and Materials Research Laboratory, University of Illinois, Urbana, Illinois 61801
(Received 9 December 1997)

Scanning tunneling microscopy is used to study the nonequilibrium surface morphology of singular and vicinal Ge(001) grown by molecular-beam epitaxy. Growth on substrates with $\approx 0.1°$ miscut produces patterns of nearly symmetrical growth mounds over a wide range of growth temperature, $60 < T < 230$ °C and film thickness, $0.5 < h < 1000$ nm. The characteristic slope or aspect ratio of the growth mounds increases with film thickness. Analysis of the onset of mound formation gives an estimate of the Ehrlich-Schwoebel length; l_{ES} is approximately equal to the surface lattice constant and independent of temperature. This small value for l_{ES} implies either a weak repulsive barrier ($\Delta E_d \sim k_B T$) at descending steps or a step-adatom attraction ($\Delta E_a > k_B T$) at ascending steps. Buffer layers grown at $T = 365$ °C on vicinal substrates (9° miscut towards [110]) show (115) facets. Low-temperature growth on vicinal surfaces (6° and 9° miscuts at $T = 155$ and 230 °C) produces highly anisotropic growth ridges oriented along the miscut direction with larger roughness amplitude and smaller in-plane length scales than mounds produced by the same growth conditions on singular substrates. At 230 °C, the slopes of the growth ridges are stabilized by the (105) surface. [S0163-1829(98)10419-8]

I. INTRODUCTION

The equilibrium morphology of most low-index crystal surfaces can be described as flat terraces separated by atomic-height steps; the average distance between steps is given by the deviation of the surface orientation from the low-index orientation, the ''substrate miscut.'' During crystal growth and thin-film deposition, however, kinetic phenomena can drive the surface out of equilibrium and produce high step densities and a rough surface morphology. Because of general interest in nonequilibrium statistical physics and the great technological relevance of this subject for controlling film and interface morphology, the evolution of surface morphology during low-temperature crystal growth has been the topic of a considerable research effort in condensed matter and materials physics.[1]

Most experiments and theory of low-temperature crystal growth are concerned with the relatively simple case of growth of elemental single crystals from so-called ''molecular beams:''[2] a flux of atoms is deposited on a single crystal substrate; the adatoms diffuse on the surface and either attach at existing steps or coalesce with other adatoms to nucleate new terraces and steps. In recent years, it has been recognized that asymmetries in the attachment of adatoms at step edges[3,4] can produce strong roughening during growth.[2,5–7] This ''diffusion bias'' for adatoms[8] destabilizes growth on singular (low-miscut) surfaces and drives the formation of patterns of ''growth mounds.'' Pattern formation during low-temperature crystal growth has been studied by analytical theory,[2,5,6,9,10] computer simulation,[9,11–13] and by experiment for a large number of systems: Cu(001),[14] GaAs(001),[5,15] Ge(001),[7] Fe(001),[16] Rh(111),[17] Si(001),[18] Ag(111),[19] and TiN(001).[20]

We have previously published our initial experiments on the growth of Ge(001) at low temperatures in a journal article[7] and conference proceedings.[21,22] In this report, we present our complete set of data for the morphology of Ge(001) using a wide range growth temperature, film thickness, and substrate miscut. In addition, we analyze the data to extract an estimate of the so-called ''Ehrlich-Schwoebel length'' l_{ES} (Ref. 10) and find that l_{ES} is comparable to the surface lattice constant. This small value for l_{ES} implies a small asymmetry in adatom attachment kinetics on Ge(001) caused by either a weak repulsive barrier at descending steps or a step-adatom attraction[12,23] at ascending steps.

II. EXPERIMENTAL DETAILS

Ge(001) films are grown on Ge(001) substrates by molecular-beam epitaxy (MBE) using electron beam evaporation. The etch pit density specified by the substrate manufacturer is 5×10^3 cm^{-2}. The miscut of 9° vicinal substrates was confirmed by x-ray diffraction. We clean the Ge(001) substrates using repeated ozone-assisted oxidation and removal of the oxide in water.[24] Samples are 1.5×1.5 cm^2 and are In bonded to a 3-in-diam Mo sample block. The final oxide layer is removed in the MBE growth chamber by annealing for 30 min at 450 °C.[24] Following oxide desorption, the surface gives a well-defined 2×1 diffraction pattern in reflection high-energy electron diffraction, but the surface morphologies have a relatively large step density and significant roughness.[7] We believe that this roughness is stabilized by residual carbon contamination since nanometer-scale roughness on a clean Ge(001) surface would decay rapidly at $T = 450$ °C.[25,26]

To produce a smooth starting surface for the low-temperature growth experiments, we deposit a 100-nm-thick Ge buffer layer at 365 °C. During Ge deposition, the chamber pressure rises to 2×10^{-9} Torr. The dominant components of the background gas are typically 1.4×10^{-9} Torr H_2, 1.4×10^{-10} Torr $CO + N_2$, and 2.5×10^{-10} Torr H_2O. For singular surfaces, scanning tunneling microscopy (STM) of the buffer layers reveals large terraces, ~ 100 nm wide, reflecting the small miscut of the wafers, $\sim 0.1°$.[7] STM images of 9° vicinal substrates show (115) facets, see discus-

0163-1829/98/57(19)/12536(8)/$15.00 © 1998 The American Physical Society

sion below. After turning off the substrate heater, the samples cool at $\sim 2\ ^\circ\mathrm{C\ sec}^{-1}$.

Growth temperatures at $T > 150\ ^\circ\mathrm{C}$ are measured using an infrared pyrometer (4.8–5.2 μm), which has been calibrated using thermocouples bonded to a Ge test sample. The emissivity used in the calibration $\epsilon \approx 0.45$ is in good agreement with the emissivity expected for Ge made opaque in the infrared by free carrier absorption $\epsilon = 1-(n-1)^2/(n+1)^2$, $n = 4$, multiplied by the transmission coefficient of the sapphire viewport at $\lambda \approx 5\ \mu$m, ≈ 0.70. We determined growth temperatures of $T = 60$ and 100 °C using a calibration of substrate heater power.

A separately pumped, ultrahigh vacuum (UHV) transfer tube connects the MBE chamber to a UHV scanning tunneling microscope. All STM images described below are obtained at room temperature at negative sample bias of ≈ 2 V and a tunneling current of ~ 100 pA. Selected samples are imaged by atomic force microscopy using commercially supplied, ''oxide-sharpened'' probe tips.

III. RESULTS AND DISCUSSION

A. Low-temperature growth on singular substrates

Figure 1 shows examples of surface morphologies created by low-temperature growth on singular surfaces. In this case, $T = 175\ ^\circ$C. For small film thickness h, see Fig. 1(a), we observe ''multilayer growth'': approximately four layers of the crystal are exposed as small area (001) terraces and islands but large-scale structures are not readily apparent. With increasing h, patterns of growth mounds appear, see Fig. 1(b), and the pattern of growth mounds become increasingly well organized, see Fig. 1(c).

We characterize these morphologies by two length scales: (i) the in-plane length scale d measured by the first peak in the height-height correlation function[27] $\langle h_i h_j \rangle$, and (ii) the amplitude of the roughness A measured by the height difference correlation function evaluated at $d/2$; i.e., $A = G^{1/2}(d/2)$ where $G(\rho) = \langle (h_i - h_j)^2 \rangle$. (In many studies of surface roughness, the feature size is measured by the position r_c of the first zero in the height-height correlation function $\langle h_i h_j \rangle$, and the roughness is measured by the surface width $W = \langle h_i^2 \rangle^{1/2}$. We prefer our measurements of d and A because we find that d and A are less sensitive to experimental artifacts than r_c and W. In most cases, however, the different methods of analysis are essentially equivalent: $d \approx 2r_c$, and $A \approx \sqrt{2}W$.)

Figure 2 summarizes the two length scales, d and A, as a function of film thickness h for five growth temperatures. Both d and A increase monotonically with increasing h—the lateral length scales coarsen and the films roughen—but the rates of coarsening and roughening are not equal. At $T > 150\ ^\circ$C, the coarsening of the lateral length scale d is initially rapid and then becomes almost independent of h for large h. The roughening rate, on the other hand, approaches a linear dependence on h; $A \propto h$ for large h.[28] Clearly, at large h, A increases much more rapidly than d, indicating that the slopes of the sides of the growth mounds are not stable.

The absence of a stable slope to the sides of the growth mounds is emphasized in Fig. 3. Histograms of local surface orientations, see Fig. 3(a), show that the most probable slope increases and that the distribution of slopes becomes narrower as growth proceeds. Since we have found that the most probable surface orientation is approximately equal to $(A/d)(360^\circ)$, we summarize this simple measure of the aspect ratio of the mounds in Fig. 3(b).

The evolution of d and A described by Figs. 2 and 3 is more complex than what is typically observed in low-temperature growth experiments and computational models, or derived by analytical theory. In most studies of growth mound evolution, both d and A increase at the same rate: $d \propto h^n$ and $A \propto h^\beta$, with a constant $n \approx \beta$ in the range $1/6 < n < 1/3$. The microscopic origin of this slope selection is somewhat controversial and is probably specific to the system under study: the formation of high index surface facets appears to be the dominate mechanism for Cu(001);[6,14] enhanced downward diffusion near descending steps, so-called ''downward funneling,'' is thought to stabilize slopes on Fe(001);[13,16] and thermal smoothing driven by step energetics or capillarity[25,26] can also provide the downward diffusion currents needed to create slope selection.

B. The Ehrlich-Schwoebel length

We now analyze the growth mound evolution described by the data in Figs. 1–3 to extract a rough estimate of the strength of the asymmetries in adatom attachment at step edges, and therefore gain a more microscopic perspective on the growth instability. Politi and Villain[10] propose the following equation to describe the surface diffusion current:

$$j = \frac{F l_{\mathrm{ES}} l_c m}{2(1+|m| l_{\mathrm{ES}})(1+|m| l_c)} + K \frac{\partial^2 m}{\partial x^2}. \tag{1}$$

The first term in Eq. (1) describes an interpolation of the expected diffusion bias current for small and large values of the step density m; F is the growth flux, and l_c is a critical length for the formation of new terraces. (In the limit of weak Ehrlich-Schwoebel barriers, l_c is approximately equal to the island separation during submonolayer deposition on large terraces[29].) Futhermore, for a $1+1$ dimensional model including repulsive barriers at descending steps,[10] the Ehrlich-Schwoebel length l_{ES} is given by

$$l_{\mathrm{ES}} = b\left(\frac{D}{D'} - 1\right), \tag{2}$$

where D is the diffusion constant for adatoms, D'/b^2 is the hopping rate for an adatom crossing a descending step, and b is the surface lattice constant.

The second term in Eq. (1) stabilizes the surface against height fluctuations of short wavelength.[10] While the origin of K is usually attributed to thermal smoothing,[30,26] Politi and Villain propose that K can also originate with the stochastic formation of new terraces. In this case, dimensional analysis gives $K \approx F l_c^4$.[10]

We evaluate the importance of thermal smoothing by comparing the increase in roughness amplitude during low-temperature growth and the decay of roughness during thermal annealing. In Fig. 4, data for the roughening rate dA/dh are plotted with the thermal smoothing rate previously measured for nanometer-scale morphologies on Ge(001):[25,26] the

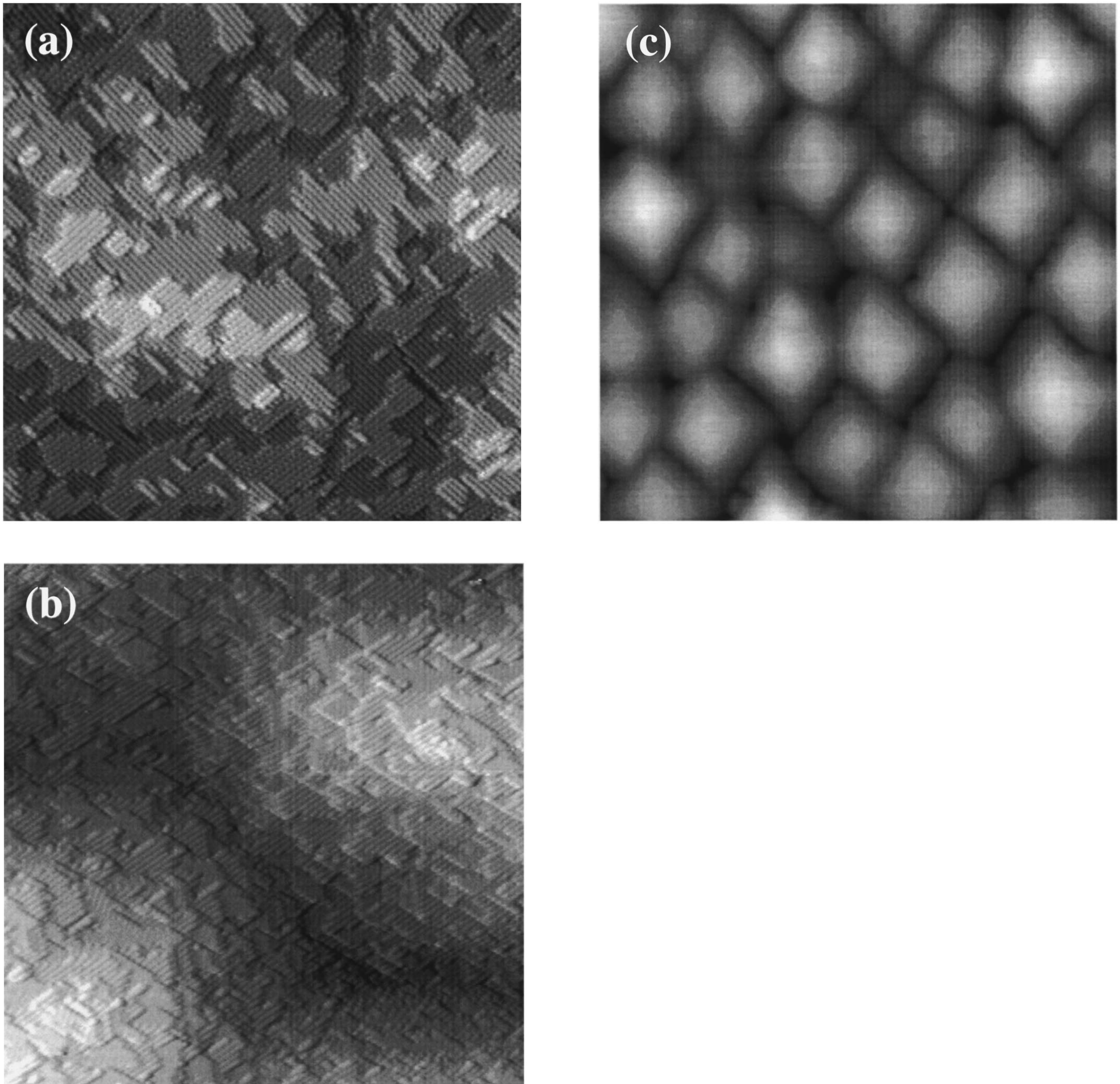

FIG. 1. Surface morphology of Ge(001) growth at 175 °C by molecular-beam epitaxy (MBE); STM images of (a) multilayer growth at film thickness $h=10$ nm; (b) growth mound formation at $h=200$ nm. The scan area of both images is 70×70 nm^2, and the images have been high-pass filtered to increase contrast to step edges. In (a), ≈ 4 ML of the crystal are exposed; in (b), the peak-to-peak change in height is ≈ 16 ML. (c) Atomic force microscopy image (AFM) of growth mounds at $h=1000$ nm. The area of the image is 700×700 nm^2 and the black-to-white range corresponds to a height change $\Delta z=15$ nm.

decay of roughness amplitude is described by a power law of the form $A(t)=A_0(1+t/\tau)^{1/2}$, where t is the annealing time, A_0 is the roughness amplitude at $t=0$, and τ is a thermally activated time constant; $\tau=\tau_0 \exp(1.7\ \mathrm{eV}/k_BT)$, $\tau_0 =C(d/2\pi)^4/(A_0/a)^2$, and $C=2\times10^{-16}\ \mathrm{sec\ nm}^{-4}$. The dashed line in Fig. 4 shows the fractional smoothing $[1-A(t)/A_0)]$ for a 10-sec anneal of patterns of etch pits ($d=65$ nm, $A_0=0.5$ nm) produced by low-energy ion sputtering; i.e., the dashed line shows an estimate of the smoothing rate for morphologies with values of d and A similar to the growth mounds. While thermal smoothing may influence mound evolution for growth at $T=230$ °C, we conclude that thermal smoothing is negligible over most of the temperature range of our experiments.

If $K\approx Fl_c^4$ in the absence of thermal smoothing, then mounds appear after a time t^*:[10]

$$t^*=\frac{1}{Fb^2}\left(\frac{l_c}{l_{\mathrm{ES}}}\right)^2. \tag{3}$$

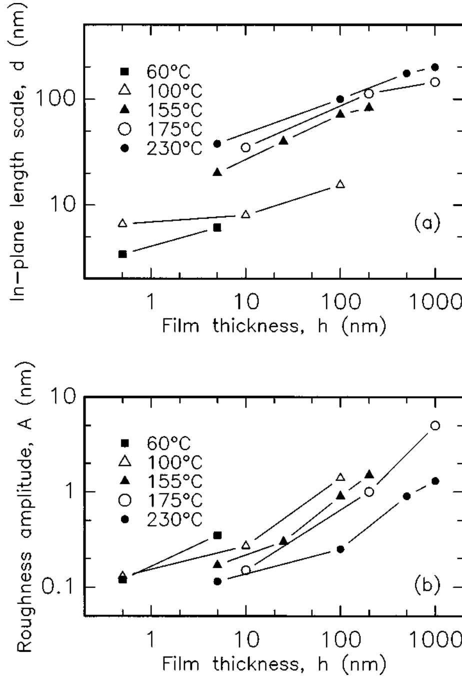

FIG. 2. (a) The characteristic in-plane length scale d of the surface morphology plotted as a function of film thickness and growth temperature; d is measured by the position of the first peak of the height-height correlation function $\langle h_i h_j \rangle$. Solid lines connect data points for the same growth temperature. (b) Roughness amplitude, $A = G^{1/2}(\rho)$, $\rho = d/2$, as a function of film thickness and growth temperature.

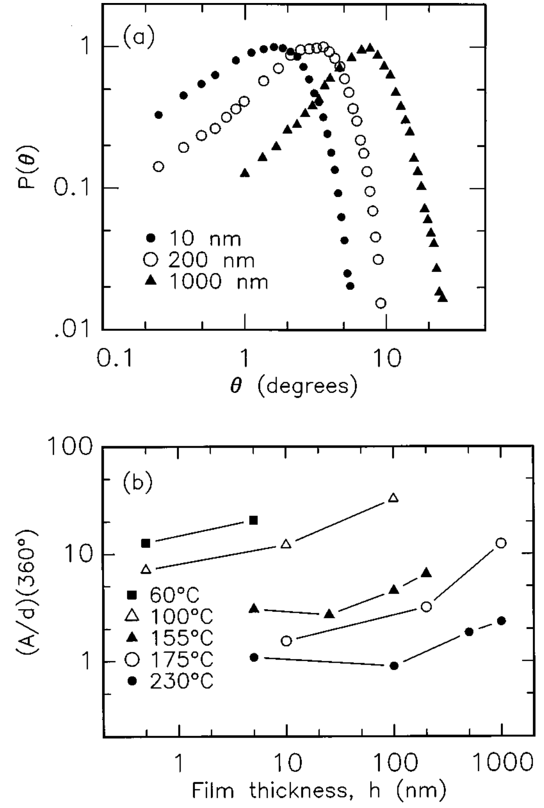

FIG. 3. (a) Histogram of local surface orientations θ for Ge(001) films grown at 175 °C on singular substrates. The local surface orientation is measured in 4×4 nm^2 areas centered on each pixel of the STM data for $h = 10$ and $h = 200$ nm and AFM data for $h = 1000$ nm. (b) Aspect ratio of the roughness (A/d) multiplied by 360°; this quantity is approximately equal to the peak of the surface orientation histograms shown in (a).

Our ''quench-and-look'' microscopy experiments do not contain sufficiently small intervals in film thickness to directly identify the onset of mound formation. But we can accurately characterize initial values of dA/dh, and since $1/(dA/dh)$ gives the number of deposited monolayers needed to create the first additional monolayer of roughness amplitude, we estimate t^* using $(dA/dh)Fb^2t^* = 1$.

To find $l_{\rm ES}$, we must first determine l_c: island densities n at a coverage of $\sim$0.3 ML were measured at $T = 100$, 155, and 230 °C. Data for $l_c = n^{1/2}$ are summarized in Fig. 5. We estimate l_c at $T = 60$ °C by extrapolating the $100 < T < 155$ °C data to lower temperatures using $l_c = (20b^2D/F)^{1/6}$ (Ref. 31) with a single free parameter, the activation energy for adatom diffusion, $E_m = 0.65$ eV. A comparison to scaled data for Si(001),[32] see Fig. 5, shows that this extrapolation is reasonable.

Figure 5 also includes data for $l_{\rm ES}$ calculated using Eq. (3) and our estimate of t^*: $l_{\rm ES} = (dA/dh)^{1/2} l_c$. The Ehrlich-Schwoebel length $l_{\rm ES}$ derived in this way is essentially independent of temperature and comparable to the surface lattice constant $b = 0.4$ nm. If the origin of $l_{\rm ES}$ is attributed to a repulsive barrier at descending steps, see Eq. (2), then the size of the barrier must be comparable to the thermal energy at the growth temperature. A fit to Eq. (2) gives $\Delta E_d = 0.024$ eV, see Fig. 5.

Politi and Villain[10] suggest that the distance between growth mounds should scale as $d \sim l_c^2/l_{\rm ES}$. This proposal is tested in Fig. 6, where we plot d scaled by $(1/b)(dA/dh)$. Since $(dA/dh) \approx (l_{\rm ES}/l_c)^2$, and $l_{\rm ES} \approx b$, our scaling is equivalent to $dl_{\rm ES}/l_c^2$. Furthermore, since the number of monolayers needed to form growth mounds scales as dA/dh, we scale the film thickness by $(dA/dh)(1/a)$; a is the monolayer step height $a = 0.14$ nm. Data for additional growth

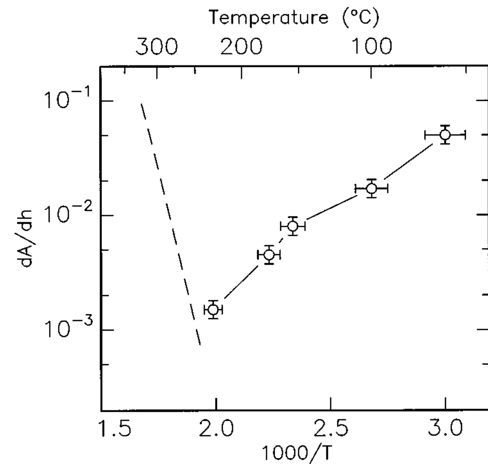

FIG. 4. Roughening rate dA/dh as a function of MBE growth temperature; dA/dh is calculated by taking finite differences $dA/dh = \Delta A/\Delta h$ for films with $A \sim 0.3$ nm but derivatives of analytical fits produce essentially the same results. The dashed line shows the fractional smoothing of nanometer-scale surface roughness ($A_0 = 0.5$ nm, $d = 65$ nm, annealing time 10 sec) as a function of annealing temperature, see Ref. 25.

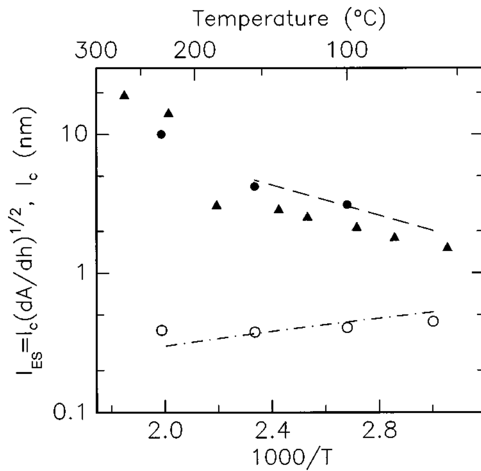

FIG. 5. Diffusion length l_c and Ehrlich-Schwoebel length l_{ES} plotted as a function of MBE growth temperature. Filled circles: $l_c = n^{1/2}$ where n is the island density for submonolayer deposition on large terraces. The dashed line shows an extrapolation to lower temperatures using $l_c = (20b^2D/F)^{1/6}$, where $D = (b^2\nu/2)\exp(-E_m/k_BT)$, $E_m = 0.65$ eV, $b = 0.4$ nm, and ν is the Debye freqency of Ge, $h\nu = k_B(375\text{ K})$. Open circles: $l_{ES} = (dA/dh)^{1/2}l_c$; data for (dA/dh) are plotted in Fig. 4. The dashed-dot line shows l_{ES} calculated using Eq. (2) with $D/D' = \exp(\Delta E_d/k_BT)$ and $\Delta E_d = 0.024$ eV. Filled triangles: $l_c = n^{1/2}$ for Si(001) from Ref. 32; to facilitate this comparison, l_c data for Si(001) have been scaled by a factor of $420^{-1/6}$ to adjust for different growth fluxes used in the Ge and Si experiments; and the temperature of the Si(001) measurements has been scaled by the ratio of the cohesive energies of Ge and Si, 0.83.

temperatures would clearly be desirable, but we believe the "data collapse" shown in Fig. 6 supports theoretical models[10] built on Eq. (1): at long times, the in-plane length scale of the growth mounds is $d \approx l_c^2/l_{ES}$.

C. Buffer layer growth on vicinal substrates

The production of flat buffer layers on vicinal substrates is not as straightforward as for singular surfaces: on 9° miscut substrates, buffer layers show faceting and the area of the facets increases with film thickness h, see Fig. 7. To measure the orientation of the facets, we calculate two-dimensional histograms of local surface orientations (data not shown); these histograms show a peak at 7.5° away from the average surface normal in the direction of the miscut. Thus, the absolute orientation of the facets is $9° + 7.5° = 16.5°$, and within experimental uncertainties of the expected orientation of a (115) surface, 15.8°. Small area STM images of the facets show a surface reconstruction that is consistent with the 1.2 nm periodicity and orientation of the geometry proposed by Ranke[33] for Si(115).[34] In the growth experiments described below, $h = 100$ nm buffer layers were used to

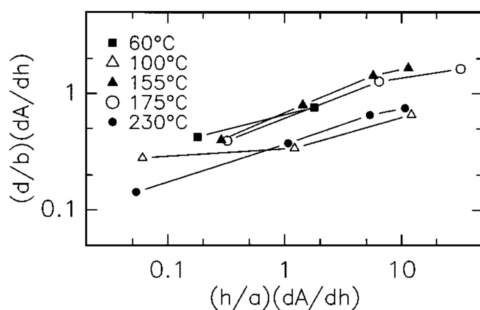

FIG. 6. Scaling of the data for the in-plane length scale d; raw data for d are plotted in Fig. 2(a); b is the surface lattice constant, $b = 0.40$ nm, and a is the monolayer step height, $a = 0.14$ nm. Data for the roughening rate dA/dh are plotted in Fig. 4.

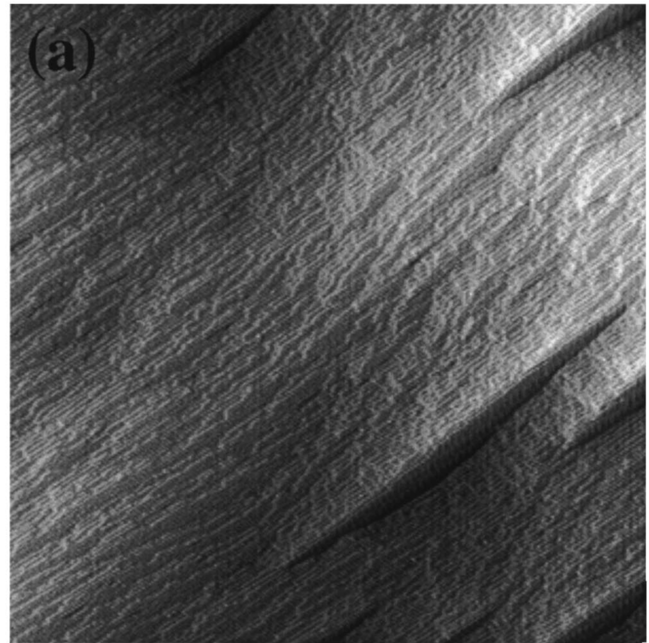

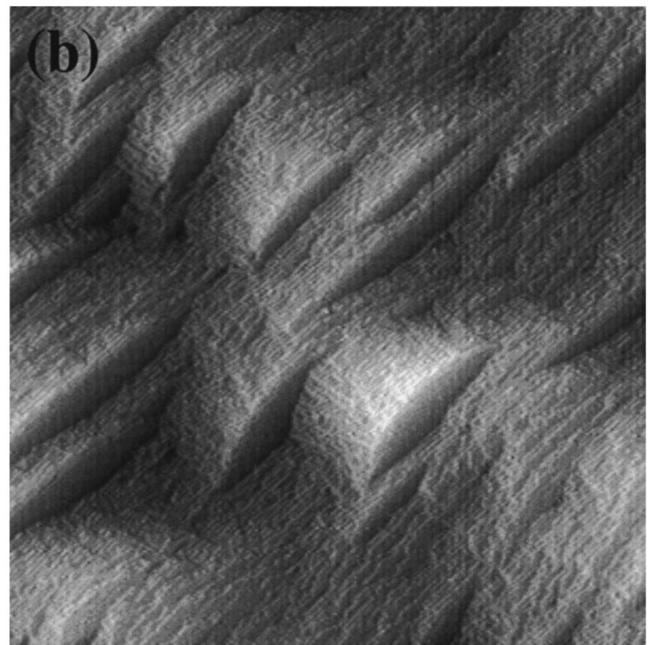

FIG. 7. STM images of buffer layers grown on Ge(001) miscut by 9° toward [011]. The growth temperature is 365 °C. (a) $h = 100$ nm; (b) $h = 300$ nm. The area of both images is $270 \times 270\text{ nm}^2$ and the images have been high-pass filtered to increase contrast to step edges and facets. The orientations of the faceted regions correspond to (115) surfaces.

minimize the influences of the (115) facets on the low-temperature growth morphology.

D. Low-temperature growth on vicinal substrates

Four combinations of growth parameters were investigated using vicinal substrates: $h = 100$ nm films grown at $T = 155$ °C and $h = 1$ μm films grown at $T = 230$ °C on 6° and 9° miscuts. [The values of the miscuts were chosen to be large compared to the mound slopes on singular surfaces at these temperatures, see Fig. 3(b).] In all cases, the surface morphology shows ''growth ridges'' oriented along the miscut direction; an example of this morphology is given in Fig. 8(a). At $T = 230$ °C, the sidewalls of the ridges are faceted. As before, we use histograms of local surface orientation to determine the orientation of the sidewall facets; the histogram for the surface shown in Fig. 8(a) peaks at 7°. Since the sidewall facets are oriented perpendicular to the miscut direction, the absolute orientation of the sidewalls is $(7^2 + 6^2)^{1/2} = 9.2°$ away from (001) and within $\approx 2°$ of the expected orientation of the (105) surface. Small area STM images of the sidewalls reveal reconstructed terraces and steps, see Fig. 8(b).

Because of the strong anisotropy of these surface morphologies, we calculate height difference correlation functions for directions parallel and perpendicular to the growth ridges. The results for all four films are given in Fig. 9. As expected based on qualitative inspections of the images, at small length scales ρ, the roughness is much smaller parallel to the growth ridges than perpendicular. Values of A and d for the growth ridges are extracted from the correlation functions for the direction perpendicular to the growth ridges and are summarized as data points in an A versus d ''phase-space,'' see Fig. 10, with comparison to results for singular substrates. Increasing the miscut from 0° to 9° reduces d by a factor of ~ 3 and increases A. The aspect ratio for growth at $T = 230$ °C appears to limited by the formation of (105) sidewall facets; growth at $T = 155$ °C does not show this limiting behavior and we conclude that (105) facets cannot stabilize the ridge morphology at $T = 155$ °C.

Our results for vicinal Ge(001) are in agreement with previous work on Si(001),[18] but not GaAs(001): for GaAs(001) growth at 600 °C, a miscut of 2° completely suppressed the formation of large-scale surface roughness.[5] Recent theory and computer simulation[9] have shown that ridge formation on vicinal surfaces is initiated by the step fingering instability studied by Bales and Zangwill,[35] and that the growth ridges eventually evolve into symmetrical growth mounds. Since we have not studied growth on vicinal substrates as a function of film thickness, we do not yet know if the predicted transition from ridges to mounds can be observed experimentally on Ge(001).

IV. CONCLUSIONS

Growth mounds produced by low-temperature growth on singular Ge(001) do not show a stable slope, implying that Ge(001) lacks a mechanism for the downward diffusion currents that are thought to produce the slope selection that has been oberved in many theoretical models and other experimental systems. Growth on highly vicinal surfaces produces a ridge morphology with greater surface roughness and smaller in-plane length scales. At a growth temperature of 230 °C, (105) facets stabilize the slopes of the sidewalls of the growth ridges.

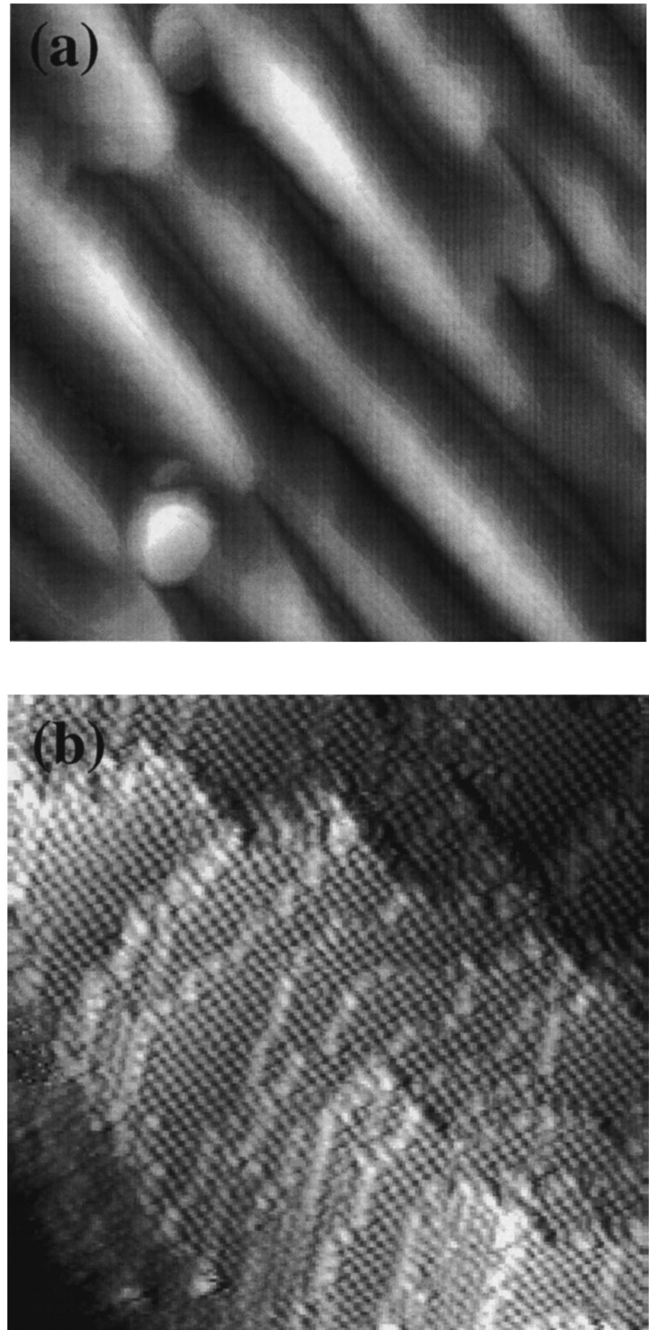

FIG. 8. STM images of faceted growth ridges grown at 230 °C on Ge(001) miscut by 6° toward [011]. The film thickness is 1000 nm: (a) scan area 540×540 nm^2; (b) image of a sidewall showing a stepped (105) surface. The scan area of (b) is 45×45 nm^2.

Measurements of the diffusion distance for adatoms l_c, combined with data for the onset of mound formation on singular surfaces, allow us to estimate the Ehrlich-Schwoebel length l_{ES}; and therefore estimate the strength of asymmetries in the kinetics for adatom attachment at step edges. Since l_{ES} is comparable to the surface lattice constant b, these asymmetries are weak. If the asymmetry is inter-

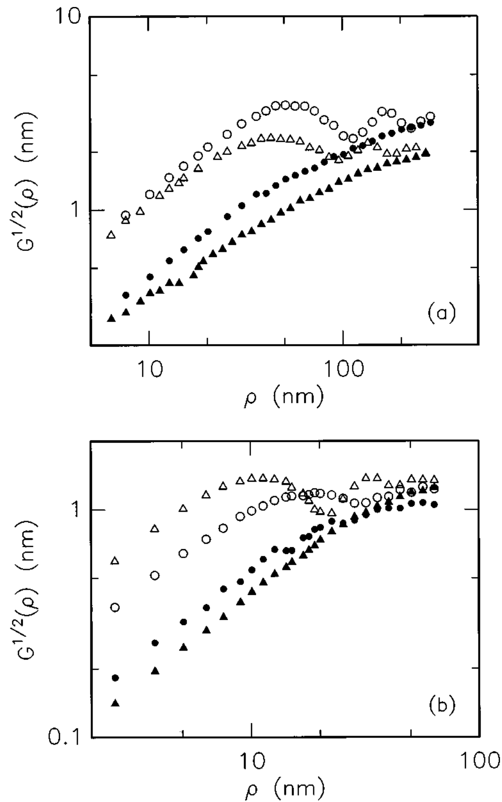

FIG. 9. Height difference correlation functions measured perpendicular (open symbols) and parallel (filled symbols) to the growth ridges produced by low-temperature MBE on vicinal Ge(001). Data for growth on 6° and 9° miscut substrates are shown as circles and triangles, respectively. (a) Growth temperature $T = 230$ °C; (b) $T = 155$ °C.

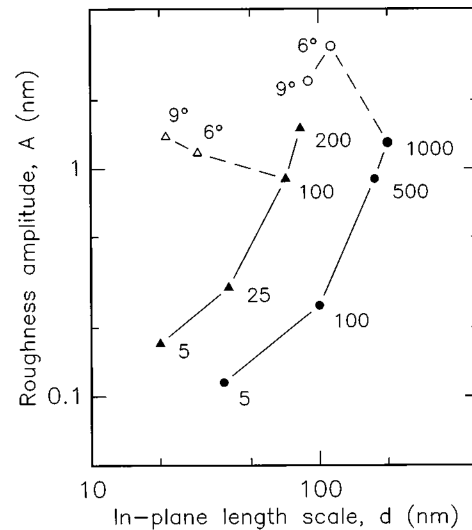

FIG. 10. A vs d "phase space" of Ge(001) morphology for growth at $T = 155$ °C (triangles) and $T = 230$ °C (circles). Filled symbols are for growth on singular surfaces and are labeled by the film thickness in nanometers. Open symbols are for growth at fixed film thickness on vicinal substrates and are labeled by the miscut angle.

preted in terms of a repulsive barrier at descending steps, then diffusion across a descending step is suppressed by only a factor of ~ 2 relative to diffusion on a terrace.

While we cannot rule out the presence of a weak barrier $\Delta E_d \sim k_B T$ at descending steps, we believe that step-adatom attraction[12,23] at ascending steps provides a more satisfactory explanation for our fundamental observation $l_{ES} \approx b$. Based on the discussion of Refs. 10 and 4, we propose that for an attractive interaction at ascending steps, l_{ES} is equal to the range over which the distortion in the potential energy landscape ΔE_a is greater than $k_B T$; for a short-range interaction, $l_{ES} \approx b$ independent of temperature. Simulations by Amar and Family[12] support this proposal: in their model, the roughening behavior is independent of the strength of the attraction for $\Delta E_a > k_B T$. Therefore, while only a narrow range of repulsive barriers with $\Delta E_d \sim k_B T$ are consistent with our experimental results, the data can be more easily explained by a wide range of attractive interactions $\Delta E_a > k_B T$.

ACKNOWLEDGMENT

This work was supported by the U.S. Department of Energy Grant No. DEFG02-96-ER45439 through the University of Illinois Materials Research Laboratory.

*Present address: WL/AADP Bldg. 620, 2241 Avionics Circle, Wright-Patterson AFB, OH 45433-7322.

†Present address: Department of Chemical Engineering and Materials Science, University of Minnesota, Minneapolis, MN 55455.

[1] Joachim Krug, Adv. Phys. **46**, 139 (1997); for a discussion of unstable MBE growth, see pp. 238–244.

[2] J. Villain, J. Phys. I **1**, 19 (1991).

[3] Gert Ehrlich and F. G. Hudda, J. Chem. Phys. **44**, 1039 (1966).

[4] Kentaro Kyuno and G. Ehrlich, Surf. Sci. **383**, L766 (1997).

[5] M. D. Johnson, C. Orme, A. W. Hunt, D. Graff, J. Sudijono, L. M. Sander, and B. G. Orr, Phys. Rev. Lett. **72**, 116 (1994).

[6] Martin Siegert and Michael Plischke, Phys. Rev. Lett. **73**, 1517 (1994); Martin Siegert and Michael Plischke, Phys. Rev. E **53**, 307 (1996).

[7] Joseph E. Van Nostrand, S. Jay Chey, M.-A. Hasan, David G. Cahill, and J. E. Greene, Phys. Rev. Lett. **74**, 1127 (1995).

[8] A diffusion bias for surface vacancies is thought to drive pattern formation during ion-etching; see, for example, S. Jay Chey, Joseph E. Van Nostrand, and David G. Cahill, Phys. Rev. B **52**, 16 696 (1995).

[9] Martin Rost, Pavel Šmilauer, and Joachim Krug, Surf. Sci. **369**, 393 (1996).

[10] Paolo Politi and Jacques Villain, Phys. Rev. B **54**, 5114 (1996).

[11] Pavel Šmilauer and Dimitri D. Vvedensky, Phys. Rev. B **52**, 14 263 (1995).

[12] Jacques G. Amar and Fereydoon Family, Phys. Rev. Lett. **77**, 4584 (1996).

[13] Jacques G. Amar and Fereydoon Family, Phys. Rev. B **54**, 14 742 (1996).

[14] H.-J. Ernst, F. Fabre, R. Folkerts, and J. Lapujoulade, Phys. Rev. Lett. **72**, 112 (1994).

[15] Joseph E. Van Nostrand, S. Jay Chey, David G. Cahill, A. E. Botchkarev, and H. Morkoç, Surf. Sci. **346**, 136 (1996).

[16] Joseph A. Stroscio, D. T. Pierce, M. D. Stiles, A. Zangwill, and L. M. Sander, Phys. Rev. Lett. **75**, 4246 (1995).

[17] F. Tsui, J. Wellman, C. Uher, and Roy Clarke, Phys. Rev. Lett. **76**, 3164 (1996).
[18] N.-E. Lee, David G. Cahill, and J. E. Greene, Phys. Rev. B **53**, 7876 (1996).
[19] W. C. Elliott, P. F. Miceli, T. Tse, and P. W. Stephens, Phys. Rev. B **54**, 17 938 (1996).
[20] Brian W. Karr, I. Petrov, David G. Cahill, and J. E. Greene, Appl. Phys. Lett. **70**, 1703 (1997).
[21] Joseph E. Van Nostrand, S. Jay Chey, and David G. Cahill, J. Vac. Sci. Technol. A **13**, 1816 (1995). In this paper, we made an error in measuring the growth temperature of the 200-nm-thick film; the correct growth temperature for the 200 nm film is 175 °C.
[22] S. Jay Chey, Joseph E. Van Nostrand, and David G. Cahill, in *Evolution of Epitaxial Structure and Morphology*, edited by A. Zangwill, D. Jesson, D. Chambliss, and R. Clarke, MRS Symposia Proceedings No. 399 (Materials Research Society, Pittsburgh, 1996), p. 221.
[23] S. C. Wang and G. Ehrlich, Phys. Rev. Lett. **70**, 41 (1993).
[24] X.-J. Zhang, G. Xue, A. Agarwal, R. Tsu, M.-A. Hasan, J. E. Greene, and A. Rockett, J. Vac. Sci. Technol. A **11**, 2553 (1993).
[25] S. Jay Chey, Joseph E. Van Nostrand, and David G. Cahill, Phys. Rev. Lett. **76**, 3995 (1996).
[26] S. Jay Chey and David G. Cahill, in *Dynamics of Crystal Surfaces and Interfaces*, edited by P. M. Duxbury and T. J. Pence (Plenum Press, New York, 1997), pp. 59–69.
[27] Jean Lapujoulade, Surf. Sci. Rep. **20**, 191 (1994); see pp. 197 and 235.
[28] An approximately linear roughening rate for Si(001) was originally observed using Ge marker layers and cross-sectional TEM; see D. J. Eaglesham, J. Appl. Phys. **77**, 3597 (1995).
[29] J. Tersoff, A. W. Denier van der Gon, and R. M. Tromp, Phys. Rev. Lett. **72**, 266 (1997).
[30] W. W. Mullins, J. Appl. Phys. **30**, 77 (1959).
[31] The factor of 20 in the relation $l_c = (20b^2 D/F)^{1/6}$ is derived from a fit to the island densities produced in computer simulations of growth; see G. S. Bales and D. C. Chrzan, Phys. Rev. B **50**, 6057 (1994).
[32] Y. W. Mo, J. Kleiner, M. B. Webb, and M. G. Lagally, Phys. Rev. Lett. **66**, 1998 (1991).
[33] W. Ranke, Phys. Rev. B **41**, 5243 (1990).
[34] For a recent discussion of microscopy results for high-index Si surfaces; see A. A. Basaki, S. C. Erwin, and L. J. Whitman, Surf. Sci. **392**, 69 (1997).
[35] G. S. Bales and A. Zangwill, Phys. Rev. B **41**, 5500 (1990).